Leveraging Bismuth Immiscibility to Create Highly Concave Noble Metal Nanoparticles

Melissa E. King[1], Yuting Xu[2], Noah L. Mason[1], Porvajja Nagarajan,[1] Fanglin Che[2*], Michael B. Ross[1*]

University of Massachusetts Lowell, Department of Chemistry, Lowell, MA 01854[1]

University of Massachusetts Lowell, Department of Chemical Engineering, Lowell, MA 01854[2]

Abstract

Noble metal nanoparticles can be designed to expose low- and high-index facets, providing precise control over the coordination environment of surface atoms. This control is essential for manipulating physical properties where surface adsorption is important, namely, sensing and catalysis. The integration of metals with differences in structure and electronics, while important for manipulating catalytic activity, does not typically yield structures with well-defined morphologies in colloidal synthesis. To create structures with unusually undercoordinated surfaces, here we leverage the immiscibility of incongruent crystal structures —Au and Bi — to synthesize and stabilize three distinct morphologies: concave tetrahedra, stella octangula (dual tetrahedron), and concave stella octangula. Structural and compositional analysis shows that only ~ 6 x10 $^{-6}$ moles of surface Bi are needed to manipulate this morphology. Moreover, we show the generalizability of this methodology by synthesizing Pd concave tetrahedra with Bi-enriched surfaces. Electrocatalytic experiments reveal that these Au architectures are highly active toward alcohol oxidation, where surface Bi is critical for alcohol adsorption. Thus, integration of immiscible elements provides a new strategy for designing highly active nanoparticles with precision.

Introduction

Nanoparticles that possess tailorable compositions and morphologies are highly relevant to the field of heterogeneous catalysis, chemical detection, and optoelectronics.[1-3] The integration of multiple elements, facets, and other structural motifs at the nanoscale can result in the emergence of new properties and functionality.[4-7] Metal nanoparticles, in particular, provide a robust and tunable platform where adsorption sites can be designed, catalytic selectivity can be enhanced, and poisoning can be mitigated.[4, 8] While the wet chemical synthesis of mono-, bi-, and multi-metallic nanoparticles possessing both low- and high-index facets is well known, the vast majority of these nanoparticles combine metals with identical or complementary crystal structures with a lattice mismatch of <10%.[9]

There are few instances of metals with large differences in lattice mismatch or dramatically different crystal structures that can be co-localized within a well-defined homogeneous nanoparticle, particularly in colloidal synthesis.[10] Combining materials that have significant lattice mismatch and/or incongruous crystal structures poses a unique synthetic challenge at the nanoscale. Small (< 10%) and large (> 10%) lattice mismatches have been incorporated in core-shell structures[11-13] and phase-separated Janus-type particles.[14] Most often, attempts to alloy or co-crystallize dissimilar metals result in metal nanoparticles with no alloying, dissolution of the as-synthesized nanoparticles due to kinetic instability, or no reaction of one or more of the metal species present in solution. Post-transition metals in particular provide opportunities for unusual main group reactivity, high energy plasmonics, and distinct bonding motifs compared to transition metals.[7, 15-17] While thermal solid-state syntheses have used antimony and bismuth to effect shape control in platinum and palladium, these syntheses require high temperatures (900 ˚C) and have

only been shown to yield one morphology (tetrahexahedra).[10] As such, these methods do not provide the precise control over nucleation and growth afforded by colloidal synthesis that allows one to realize highly distinct faceting and concavity essential for increased catalytic activity, poison-resistant surfaces, and tailorable compositions and geometries.[18]

Within the domain of colloidal synthesis, however, strategic manipulation of a lattice mismatch that is >10% or incongruous crystal structures, such as face-centered cubic (fcc) and rhombohedral (rhl), could lead to new nanoparticles with complex surfaces and high-index facets. By coupling known wet chemical methods, such as galvanic exchange or sequential co-reduction, with mechanistic insights about nanoparticle growth, co-localized multimetallic nanoparticles can be made with precision. For example, tetrahedral structures composed of fcc metals, such as gold, require a symmetry-breaking event for formation, making it difficult to access via standard wet-chemical synthetic methods.[19, 20] Exploiting these existing synthetic strategies for new classes of metallic elements would provide new avenues for manipulating nanoparticle symmetry, thereby broadening the scope of accessible nanomaterials with designed surfaces.

Herein, we report a strategy that leverages the incorporation of bismuth, which typically adopts a rhombohedral lattice, with the fcc gold or palladium metals to yield nanoparticles that have underlying tetrahedral geometries and highly concave surface features. This method leverages wet chemical means and exploits the incongruous crystal structures of the gold and bismuth precursors to synthesize three distinct, uniform, and highly concave nanoparticles: concave tetrahedra, stella octangula, and concave stella octangula. Structural characterization reveals that Bi remains on the surface after stable nanoparticles are synthesized, while temporal elemental analysis of the synthesis reveals that the rate and relative proportions of co-crystallization of these metals in the initial minutes is critical for generating the final crystal

morphology. We find that the highly concave Bi-rich nanoparticle surface is active toward electrochemical glucose and ethanol oxidation, which computational modeling suggests is in part due to the relatively oxophilic Bi atoms enhancing the coordination of alcohols to the surface. This strategy provides a foundation for the synthesis of a library of previously unattainable metal nanoparticles that have useful chemical, optical, and electronic properties regardless of the incongruity of their crystal structures.

Results and Discussion

The incorporation of bismuth into the colloidal synthesis of gold nanoparticles yields three distinct morphologies that are majority gold with trace amounts of bismuth: concave tetrahedra, stella octangula, and concave stella octangula (**Figure 1A**). In a typical synthesis, Au seed nanoparticles were synthesized by adding 250 μL of tetrachloroauric acid ($HAuCl_4$) to 10 mL of 100 mM cetyltrimethylammonium chloride (CTAC) containing 200 μL of 1 M hydrochloric acid (HCl). Rapid reduction of Au is initiated by injection of 600 μL of freshly prepared 10 mM sodium borohydride ($NaBH_4$) with vigorous stirring for two minutes which produces small seed particles. After a two-hour aging period, the as prepared seeds were serially diluted and injected in 100 μL aliquots to prepared growth solutions containing at least 500 μL of 10 mM $HauCl_4$, 75 μL of 100 mM nitric acid (HNO_3), 70 μL of 10 mM bismuth nitrate ($Bi(NO_3)_3$, in 10 mL of 100 mM CTAC (**Methods**). Scanning electron microscopy (SEM) and transmission electron microscopy (TEM) revealed the synthesis of three highly concave uniform nanocrystals (**Figure 1B-D)**.

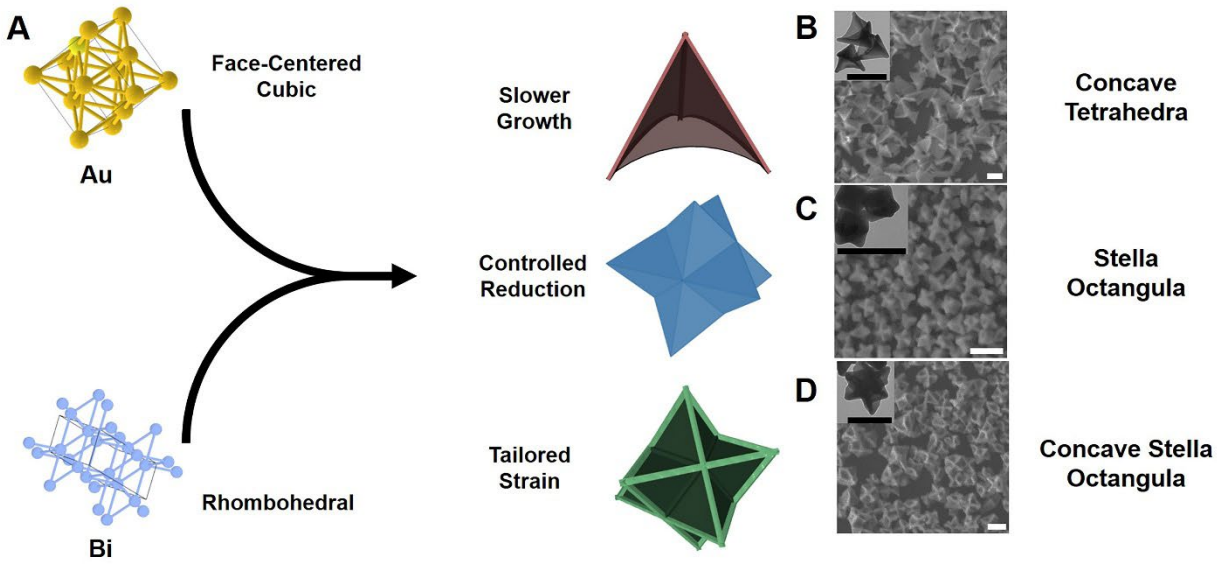

Figure 1. Bi-Directed Synthesis of High Index Anisotropic Nanoparticles: (A) Scheme of individual reaction pathways and the resultant morphologies (left). SEM and TEM micrographs of concave tetrahedra (B), stella octangula (C), and concave stella octangula (D). Scale bars: 100 nm

While the incorporation of bismuth is the most critical step in achieving these morphologies, the independent manipulation of growth rate, nanoparticle size, and metal ion reduction allowed for the differentiation in the morphologies (**Figure 1, Methods**) The first observed structure possesses a concave tetrahedral morphology. The concave tetrahedra is a well-formed shape that is almost entirely hollow, has observable curvature at the edges, and possesses a three-fold access of symmetry (**Figure 1B**). The incorporation of low concentrations of nitric acid into this growth solution improves overall nanoparticle homogeneity and increases concavity of the overall structure (**Figure S1**). Without the incorporation of nitric acid, a dual population of nanoparticles is observed, with both the concave tetrahedral geometry and a concave rhombohedral counterpart being present (**Figure S2**). While the TEM micrographs suggest that this concave

tetrahedral morphology is smooth on the outside, closer inspection of the collected SEM images reveal concavity at the surface of the nanoparticle (**Figure 1B, inset**). The tetrahedral morphology is of interest because the significant degree of concavity and surface strain is unusual to this degree in fcc metals.

The stella octangula, the second distinct structure observed, has deep grooves at the surface which form an X pattern on one side and are seemingly the twinned counterpart to the tetrahedral structure (**Figure 1C**).[18, 21-23] Looking down the three-fold axis of the stella octangula, there is the same observable point in the concave tetrahedra structure (**Figure S3**). There are three points facing outward with flat surfaces which would be the bottom of a second tetrahedral structure if they were faced in opposite directions. To realize stella octangula, low micromolar concentrations of sodium bromide, a known kinetic control reagent, were incorporated, changing the rate of co-crystallization and thus the resultant morphology (**Figure S4**).[24]

The concave stella octangula (**Figure 1D**) possesses deep wells at the surface with a solid core and mimics the stella octangula morphology with an X on one side and a three-fold axis on the other (**Figure S3**). The significantly increased concavity of these nanoparticles was achieved by decreasing the number of available seeds (nucleation sites), thus producing larger nanoparticles. These larger nanoparticles have a greater radius of curvature which enables the stabilization of high energy surface features (**Figures 1, S4**).[25] The highly strained and curved surface features can be seen in the enlarged TEM micrographs (**Figure 2A-C**), which are not observable in the absence of Bi (**Figure S5**). STEM mapping provides further corroboration of dilute Bi at each morphologies surface (**Figure 2A-C, insets**).

To better understand the role of Bi in the synthesis, extensive structural characterization was performed. X-ray diffraction (XRD) shows that the final nanoparticle morphology has the

characteristic fcc pattern expected for a Au nanocrystal (**Figure S6**), without reflections for rhl Bi, Bi oxide (Bi_2O_3), or Bi hydroxide ($Bi(OH)_3$). To elucidate the role of bismuth in the stabilization of the highly-strained nanoparticle morphologies, X-ray photoelectron spectroscopy (XPS), inductively coupled plasma-mass spectrometry (ICP-MS), and high-angle annular dark-field scanning transmission electron microscopy (HAADF-STEM) coupled with energy dispersive X-ray spectroscopy (EDS) were used. XPS reveals typical gold features (Au 4f) at ~ 85 eV and 88.5 eV in the collected spectra for each of the morphologies with somewhat oxidized Bi (Bi 4f) at ~ 158 eV and 163 eV features (**Figure 2E, F)**.

Semi-quantitative XPS analysis reveals that the percentage of Bi at the nanoparticle surface is 1.9, 0.2, and < 0.1 % for the concave tetrahedra, stella octangula, and concave stella octangula, respectively. Meanwhile, ICP-MS quantification shows that the concave tetrahedra, stella octangula, and concave stella octangula have 0.33, 0.30, and 0.10 % Bi, respectively (**Table S1**). When taken together, the combined ICP-MS and XPS measurements indicate that the available bismuth within each of these morphologies is limited to the surface of the nanoparticle and that there is not significant incorporation into the bulk. Given that the XRD patterns show no significant change in the fcc lattice, any perturbations due to Bi incorporation seem to be localized at the surface.

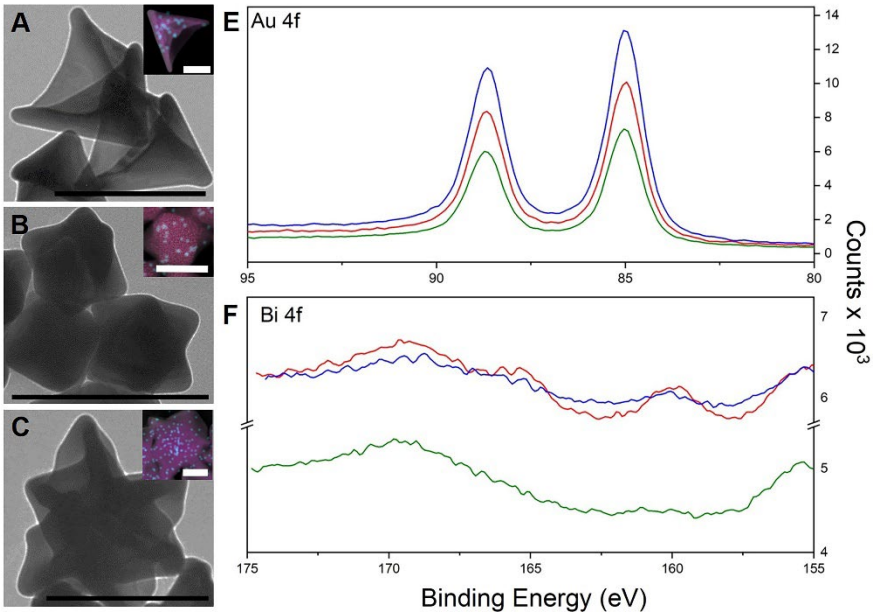

Figure 2. Structural and Compositional Characterization of Nanoparticle. TEM micrographs and HAADF STEM mapping (inset; Au elemental signature is red and Bi is blue) of concave tetrahedra (A), stella octangula (B), and concave stella octangula (C). Scale bars: 200 nm (inset is 100 nm). XPS for Auf (E) and Bi 4f (F) of concave tetrahedra (red), stella octangula (blue), and concave stella octangula (green).

While the analysis of the final nanocrystals provides some context for the role of Bi as a surface species, it only samples the final product and cannot give insight into the kinetics of growth and metal deposition. Given that XPS revealed dilute (< 2%) bismuth present at the surface upon completion of the reaction, temporally resolved experiments were carried out to better determine the Bi throughout the shape formation process. Time-stopped ICP-MS (**Figure 3, Table S2**) was carried out using a chelating agent (Bis(p-sulfonatophenyl)phenylphosphine dihydrate dipotassium salt (BSPP)) to halt growth while electron microscopy was used to monitor the reaction structurally. These results show that early incorporation of bismuth is critical to the

development of the final nanoparticle morphologies (**Figure 3, S7, Table S2**). The nanoparticle morphology is well-defined after five minutes. Initial concentrations of bismuth are significantly greater for the concave tetrahedra (~ 40%) whereas the stella octangula and concave stella octangula contain ~ 6 and 3.5%, respectively (**Table S2**). Moreover, the depth of concavity seems to be related to the relative amounts of incorporated bismuth during early time points.

The high concentration of the Bi in the concave tetrahedra suggests a co-crystallization followed by galvanic exchange as the reaction proceeds to yield a hollowed structure with Bi stabilized at the surface. The formation of the stella octangula and concave stella octangula morphologies evolves through later incorporation of Bi. The stella octangula reached a maximum Bi concentration of ~ 11% by 30 seconds with the initial delay in bulk reduction of Bi being driven by the incorporation of Br into the growth solution. The concave stella octangular nanoparticles had both Br and a reduced number of available nucleation sites with the greatest incorporation of Bi reaching ~ 18% by 2 minutes before a depletion of the Bi content. Each of these nanoparticles structures also has Bi stabilized at strained surfaces. It should be noted that greater concavity is exhibited by the concave stella octangular morphology which incorporates a similar amount of Bi into the growing crystal as its concave tetrahedral counterpart (~ 19% at 30 seconds).

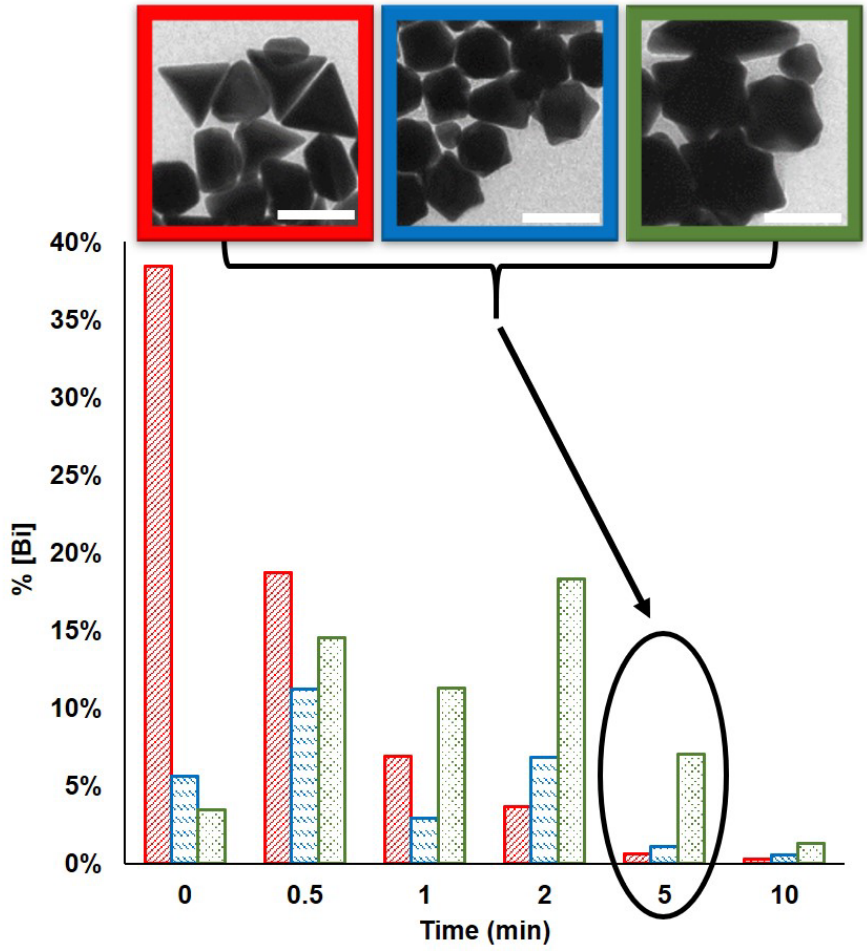

Figure 3. Kinetics of Bi Incorporation and Shape Evolution: Nanoparticle formation in the first ten minutes of the growth period of concave tetrahedra (red), stella octangula (blue), and concave stella octangula (green) with respect to bismuth incorporation. Scale bars 100 nm.

To show that this method is generalizable, palladium was selected as a second fcc metal for investigation. In a similarly structured seed-mediated colloidal synthesis (see detailed methods), palladium-bismuth concave tetrahedra were synthesized that possess the same global nanoparticle morphology (**Figure 4, S8**) as the gold counterpart. Here, optimization of the pH (by controlling the addition of HNO_3, **Figure S9**) was key to realizing uniform concave tetrahedra.

XRD (**Figure S10**) shows only the bulk fcc reflections for Pd, suggesting that there is no detectable bulk Bi or bismuth oxide. XPS shows that both palladium and bismuth are confirmed on the nanoparticle surface, with palladium peaks (Pd 3d) at ~ 332 and 337 eV and bismuth peaks (Bi 4f) at ~ 159 and 164 eV (**Figure 4)**. Interestingly, the incorporation of bismuth with palladium stabilizes at higher concentrations on the surface of the tetrahedral structure compared to the analogous gold tetrahedra. The compositional analysis of these nanoparticles shows ~ 13% bismuth at the surface of the palladium nanoparticles, which is ~ 6.5 times greater than its gold counterpart, despite the shared morphological traits and overall crystal packing order (fcc) of gold and palladium. Thus, this strategy for the synthesis of undercoordinated anisotropic nanoparticles using disparate crystal structures appears to be generalizable.

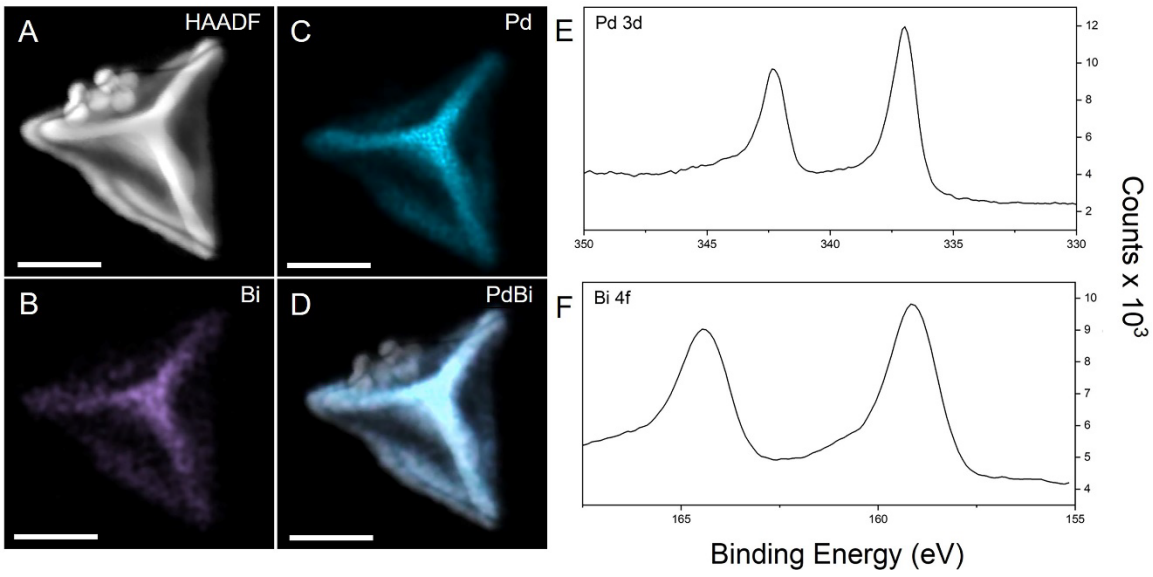

Figure 4. Bi-Directed Synthesis of Palladium Concave Tetrahedra: HAADF-STEM images (left) (A) HAADF image (B) Bi elemental map (C) Pd elemental map (D) Pd/Bi combined elemental map. Scale bars are 100 nm. XPS for palladium (E) and bismuth (F).

The highly strained Bi enriched surfaces of these architectures make them attractive for catalytic investigations; Au in particular can be highly active for alcohol and glucose oxidation in basic conditions without significant poisoning or deactivation that is common in other reaction conditions.[26-28] Meanwhile, the plasmonic properties of nanostructured Au can accelerate rates and lower overpotentials for electrochemical reactions.[29, 30] Photoelectrocatalytic alcohol oxidation experiments were carried out using an in-house built LED light source in a two-sided electrochemical cell with each catalyst drop-cast on a glassy carbon electrode with equivalent mass loading (~ 100 μg). The concave tetrahedra, stella octangula, and concave stella octangula were tested for their efficacy in alcohol oxidation in comparison with concave cubic gold nanoparticles as a control.[31] All selected shapes were ~ 100 nm in along their primary axis and confirmed to be plasmonic by UV-visible spectroscopy (**Figure S11**). The concave cubes were chosen because they have known high-index faceting, {720} and possess dilute bimetallic Ag-Au surfaces, in contrast with the Bi-Au surfaces synthesized in this work.

Both ethanol (**Figure 5A**) and glucose (**Figure S12**) oxidation were investigated in basic electrolyte. Cyclic voltammograms (CV) reveal high activity and low overpotential onsets of ethanol oxidation in comparison with the concave cubic nanoparticles (**Figure 5A**). Because all of these nanoparticles are robust plasmonic light absorbers (**Figure S11**), their photo-enhanced activity was also quantified (**Figure 5B**). In all cases, optical excitation enhanced the activity toward ethanol oxidation compared to the dark condition (**Figure 5C**). Control experiments using only basic electrolyte showed little to no optical enhancement or activity, further supporting that this is a plasmonic enhancement of electrocatalysis rather than simple photocharging (**Figures S13 and S14**). Enhancements in activity for glucose oxidation is observed for all shapes. Here the stella

octangula and concave stella octangula have the most pronounced enhancement in light-dark activity. (**Figures S12 and S14**).

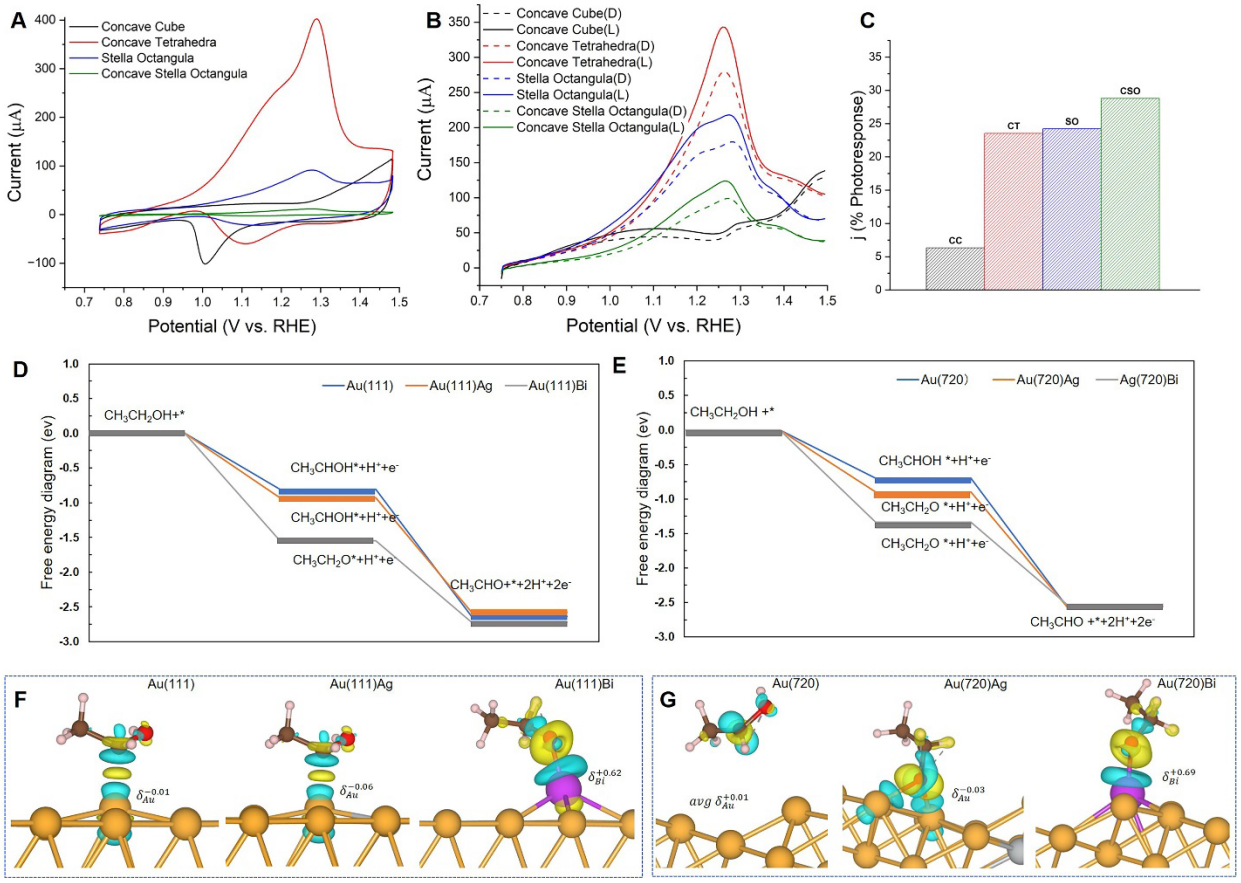

Figure 5: Bi-Enhanced Alcohol Oxidation on Gold Nanoparticles. (A) cyclic voltammograms of ethanol in NaOH electrolyte for the gold nanoparticles of interest. (B) Linear sweep voltammograms with optical excitation (solid) and dark (dashed) in the same conditions as (A). (C) Optical enhancement factors for photoelectrocatalysis at 1.26 V vs. RHE. Calculated catalytic pathways on the low-index (D) and high-index (E) surfaces for Au, Au-Ag, and Au-Bi surfaces. Adsorption and coordination geometries of $*CH_3CH_2O$ on the low-index (F) and high-index (G) facets.

Density functional theory (DFT) calculations were performed to understand the differences in electrocatalytic activity of the Ag- and Bi-enriched gold surfaces for ethanol oxidation.[32] Specifically, low index (111) and high index (720) facets were compared for the ethanol oxidation process (**Figures S15-18, Table S3**). The (111) facet was chosen because it is the most thermodynamically favorable facet for Au; while the (720) facet is a concanve facet observed experimentally in Ag-coated Au concave cubic nanoparticles.[31] Two pathways for ethanol oxidation were examined (**Figure S19)** with different intermediates for the two oxidation elementary steps.[33-35] In the first pathway, the first H atom is lost from the α-C atom, resulting in the formation of $*CH_3CHOH$. Then, a second H is removed from the oxygen atom, leading to the formation of CH_3CHO. The second pathway involves the removal of the H atom from the hydroxyl. This leads to the formation of an intermediate $*CH_3CH_2O$. Subsequently, this intermediate undergoes further transformations, ultimately resulting in the formation of CH_3CHO. Adsorption energies were calculated along each pathway to generate the most favorable thermodynamic free energy diagrams for each examined surface (**Figure 5D, E, Figures S20-S50**). Mechanistically, it is seen that Bi at the Au surface reduces the adsorption energy of $*CH_3CH_2O$ compared to both Ag-enriched and the bare Au surface (**Figure 5D, E**). Visually, it is observed that the presence of Bi enables a strong Bi-O bond between the key intermediate $*CH_3CH_2O$ and the Bi-enriched Au surface (**Figure 5F, G**), in contrast with the favored parallel adsorption for Ag-enriched Au and bare Au (**Figure 5F, G**). Bader charge analysis (**Figure 5F, G**) reveals that there is much greater charge transfer between the key intermediate $*CH_3CH_2O$ and the Bi atoms than with Ag or Au atoms.[36, 37] Charge analysis further supports that the oxygen affinity of Bi enhances the ethanol oxidation process.

Conclusion

In two fcc metals— Au and Pd— the use of immiscible rhombohedral Bi is shown to facilitate the growth of highly concave nanocrystals in colloidal synthesis. This is highly tunable in Au systems in particular, where three unique nanoscale morphologies are realized: concave tetrahedra, stella octangula, and concave stella octangula. The as-synthesized nanoparticles are optically and catalytically active with the stabilization bismuth at the surface of these highly strained structures contributing to their overall applicability for enhanced alcohol oxidation reactions. This wet-chemical synthetic strategy for the synthesis of multimetallic nanoparticles is advantageous because it occurs under mild conditions in an aqueous based growth solution; its seeded nature affords precise control over the reactants, kinetics, and growth steps.

This method introduces a new strategy and opportunity for realizing multimetallic nanoparticles, in addition to new questions relating to the core symmetry-breaking and shape-forming events in seeded growth. Early incorporation of Bi into the seeded synthesis is critical for leading to the realization of these shapes, thus future higher resolution electron microscopy and advanced spectroscopy are needed to understand the symmetry-breaking events. While both Au and Pd nanoparticles were synthesized using Bi as a shape-directing agent, more work is needed to reveal how general this approach can be. The substitution of palladium yielding the same concave tetrahedral morphology that Au made suggests that the inherent immiscibility and underlying individual crystal structures have a greater impact on final morphology than the individual components. There are also many other potential elements that could be used to direct the final shapes besides Bi, post-transition metals are a particularly interesting class due to their highly distinct structural, electronic, plasmonic properties compared to the rest of the transition

metals.[17] The ability to integrate immiscible metal components to form surface alloys of highly desirable combinations based on their electronic, optical, and combined catalytic contributions regardless of crystal habit significantly expands the library of available materials.

Author Information:

Corresponding Author:

E-mail: Michael_ross@uml.edu (M.B.R.)

Fanglin_che@uml.edu (F.C.)

ORCID:

Michael B. Ross 0000-0002-2511-0594

Melissa E. King 0000-0002-4917-9684

Noah L. Mason 0000-0003-1645-9337

Fanglin Che 0000-0001-5109-8296

Conflicts of interest

The authors declare no competing financial interests.

Acknowledgements

This work relates to Department of Navy award N00014-20-1-2858 and N00014-22-1-2001 issued by the Office of Naval Research. The United States Government has a royalty-free license throughout the world in all copyrightable material contained herein. Characterization was supported in part by the National Science Foundation Major Research Instrumentation program under Grant 2216240. This material was also supported by the University of Massachusetts Lowell and the Commonwealth of Massachusetts. We are grateful to the UMass Lowell Core Research Facilities, the Yale West Campus Materials Characterization Core for the use of the PHI Versaprobe II, and to the Yale YINQE facility for the use of the FEI Tecnai Osiris. Y.X. and F.C. also acknowledge computational resources provided by ACCESS Maximize Project No. CHM220016, ACCESS Accelerate Project No. CHE200083, and ACCESS Explore Project No. CHE220075. M.E.K. gratefully acknowledges support from the American Association of University Women American Postdoctoral fellowship. N.L.M. gratefully acknowledges support through the Kennedy Colleges of Science KCS Science Scholars program and NESACS Norris-Richards Fellowship from the Northeastern Section of the American Chemical Society.

Author Contributions

M.E.K. and M.B.R. designed the systems, collected and analyzed data, validated the methods and analysis, and wrote the manuscript. F.C. and Y.X. designed and performed calculations and wrote the manuscript. N.L.M. collected and analyzed data and wrote the manuscript. P.N. wrote the manuscript.

Declaration of Interests

The authors declare no competing interests.

References

1. Linic, S.; Christopher, P.; Xin, H.; Marimuthu, A., Catalytic and Photocatalytic Transformations on Metal Nanoparticles with Targeted Geometric and Plasmonic Properties. *Accounts of Chemical Research* **2013,** *46* (8), 1890-1899.

2. Li, P.; Bi, J.; Liu, J.; Wang, Y.; Kang, X.; Sun, X.; Zhang, J.; Liu, Z.; Zhu, Q.; Han, B., p–d Orbital Hybridization Induced by p-Block Metal-Doped Cu Promotes the Formation of C2+ Products in Ampere-Level CO2 Electroreduction. *Journal of the American Chemical Society* **2023,** *145* (8), 4675-4682.

3. Li, T.; Zhu, X.; Hai, X.; Bi, S.; Zhang, X., Recent Progress in Sensor Arrays: From Construction Principles of Sensing Elements to Applications. *ACS Sensors* **2023**.

4. Zhang, S.; Yi, X.; Hu, G.; Chen, M.; Shen, H.; Li, B.; Yang, L.; Dai, W.; Zou, J.; Luo, S., Configuration regulation of active sites by accurate doping inducing self-adapting defect for enhanced photocatalytic applications: A review. *Coordination Chemistry Reviews* **2023,** *478*, 214970.

5. Vartanian, A., Better catalysts in a (nut)shell. *Nature Reviews Materials* **2023,** *8* (4), 222-222.

6. Zhou, M.; Li, C.; Fang, J., Noble-Metal Based Random Alloy and Intermetallic Nanocrystals: Syntheses and Applications. *Chem. Rev.* **2020,** *121* (2), 736-795.

7. King, M. E.; Fonseca Guzman, M. V.; Ross, M. B., Material strategies for function enhancement in plasmonic architectures. *Nanoscale* **2022,** *14* (3), 602-611.

8. Higareda, A.; Rosas, G.; Pérez, R.; Esparza, R., Characterization and Electrocatalytic Features of PtPd and PdPt Bimetallic Nanoparticles for Methanol Electro-oxidation. *ChemNanoMat* **2021,** *7* (8), 958-965.

9. Jung, H.; King, M. E.; Personick, M. L., Strategic synergy: advances in the shape control of bimetallic nanoparticles with dilute alloyed surfaces. *Current Opinion in Colloid & Interface Science* **2019,** *40*, 104-117.

10. Huang, L.; Liu, M.; Lin, H.; Xu, Y.; Wu, J.; Dravid, V. P.; Wolverton, C.; Mirkin, C. A., Shape regulation of high-index facet nanoparticles by dealloying. *Science* **2019,** *365* (6458), 1159-1163.

11. Jocelyn, T.; Leonardi, A.; Sang, X.; Koczkur, K. M.; Unocic, R. R.; Engel, M.; Skrabalak, S. E., Effect of lattice mismatch and shell thickness on strain in core@shell nanocrystals. *Nanoscale Advances* **2020,** *2* (3), 1105-1114.

12. Li, G. G.; Blom, D. A.; Pandey, S.; Koch, R. J.; Misture, S. T.; Phillpot, S. R.; Wang, H., Overcoming the Interfacial Lattice Mismatch: Geometry Control of Gold–Nickel Bimetallic Heteronanostructures. *Particle & Particle Systems Characterization* **2018,** *35* (5), 1700361.

13. Lim, B.; Kobayashi, H.; Yu, T.; Wang, J.; Kim, M. J.; Li, Z.-Y.; Rycenga, M.; Xia, Y., Synthesis of Pd−Au Bimetallic Nanocrystals via Controlled Overgrowth. *Journal of the American Chemical Society* **2010,** *132* (8), 2506-2507.

14. Liu, J.; Zhang, J., Nanointerface Chemistry: Lattice-Mismatch-Directed Synthesis and Application of Hybrid Nanocrystals. *Chemical Reviews* **2020,** *120* (4), 2123-2170.

15. Leitao, E. M.; Jurca, T.; Manners, I., Catalysis in service of main group chemistry offers a versatile approach to p-block molecules and materials. *Nature Chemistry* **2013,** *5* (10), 817-829.

16. Melen, R. L., Frontiers in molecular p-block chemistry: From structure to reactivity. *Science* **2019,** *363* (6426), 479-484.

17. Fonseca Guzman, M. V.; King, M. E.; Mason, N. L.; Sullivan, C. S.; Jeong, S.; Ross, M. B., Plasmon manipulation by post-transition metal alloying. *Matter* **2023,** *6* (3), 838-854.

18. Robertson, D. D.; Personick, M. L., Growing Nanoscale Model Surfaces to Enable Correlation of Catalytic Behavior Across Dissimilar Reaction Environments. *Chem. Mater.* **2019,** *31* (4), 1121-1141.

19. Zheng, Y.; Liu, W.; Lv, T.; Luo, M.; Hu, H.; Lu, P.; Choi, S.-I.; Zhang, C.; Tao, J.; Zhu, Y.; Li, Z.-Y.; Xia, Y., Seed-Mediated Synthesis of Gold Tetrahedra in High Purity and with Tunable, Well-Controlled Sizes. *Chemistry – An Asian Journal* **2014,** *9* (9), 2635-2640.

20. Sun, M.; Cheng, Z.; Chen, W.; Jones, M., Understanding Symmetry Breaking at the Single-Particle Level via the Growth of Tetrahedron-Shaped Nanocrystals from Higher-Symmetry Precursors. *ACS Nano* **2021,** *15* (10), 15953-15961.

21. Smith, J. D.; Scanlan, M. M.; Chen, A. N.; Ashberry, H. M.; Skrabalak, S. E., Kinetically Controlled Sequential Seeded Growth: A General Route to Crystals with Different Hierarchies. *ACS Nano* **2020,** *14* (11), 15953-15961.

22. Lofton, C.; Sigmund, W., Mechanisms Controlling Crystal Habits of Gold and Silver Colloids. *Adv. Funct. Mater.* **2005,** *15* (7), 1197-1208.

23. Elechiguerra, J. L.; Reyes-Gasga, J.; Yacaman, M. J., The role of twinning in shape evolution of anisotropic noble metal nanostructures. *J. Mater. Chem.* **2006,** *16* (40).

24. Langille, M. R.; Personick, M. L.; Zhang, J.; Mirkin, C. A., Defining Rules for the Shape Evolution of Gold Nanoparticles. *J. Am. Chem. Soc.* **2012,** *134* (35), 14542-14554.

25. King, M. E.; Personick, M. L., Bimetallic Nanoparticles with Exotic Facet Structures via Iodide-Assisted Reduction of Palladium. *Particle & Particle Systems Characterization* **2017,** *34* (5).

26. Rodriguez, P.; Koper, M. T. M., Electrocatalysis on gold. *Phys. Chem. Chem. Phys.* **2014,** *16* (27), 13583-13594.

27. Xu, H.; Song, P.; Yan, B.; Wang, J.; Guo, J.; Du, Y., Surface-Plasmon-Enhanced Photo-electrocatalytic Ethylene Glycol Oxidation Based on Highly Open AuAg Nanobowls. *ACS Sustainable Chemistry & Engineering* **2018,** *6* (3), 4138-4146.

28. Yan, S.; Zhang, S.; Lin, Y.; Liu, G., Electrocatalytic Performance of Gold Nanoparticles Supported on Activated Carbon for Methanol Oxidation in Alkaline Solution. *J. Phys. Chem. C* **2011,** *115* (14), 6986-6993.

29. Wang, C.; Nie, X.-G.; Shi, Y.; Zhou, Y.; Xu, J.-J.; Xia, X.-H.; Chen, H.-Y., Direct Plasmon-Accelerated Electrochemical Reaction on Gold Nanoparticles. *ACS Nano* **2017,** *11* (6), 5897-5905.

30. Wilson, A. J.; Mohan, V.; Jain, P. K., Mechanistic Understanding of Plasmon-Enhanced Electrochemistry. *J. Phys. Chem. C* **2019,** *123* (48), 29360-29369.

31. Zhang, J.; Langille, M. R.; Personick, M. L.; Zhang, K.; Li, S.; Mirkin, C. A., Concave Cubic Gold Nanocrystals with High-Index Facets. *J. Am. Chem. Soc.* **2010,** *132* (40), 14012-14014.

32. Kresse, G.; Hafner, J., Ab initiomolecular dynamics for liquid metals. *Physical Review B* **1993,** *47* (1), 558-561.

33. Wang, H.-F.; Liu, Z.-P., Comprehensive Mechanism and Structure-Sensitivity of Ethanol Oxidation on Platinum: New Transition-State Searching Method for Resolving the Complex Reaction Network. *J. Am. Chem. Soc.* **2008,** *130* (33), 10996-11004.

34. Wang, E. D.; Xu, J. B.; Zhao, T. S., Density Functional Theory Studies of the Structure Sensitivity of Ethanol Oxidation on Palladium Surfaces. *J. Phys. Chem. C* **2010,** *114* (23), 10489-10497.

35. Wu, R.; Wang, L., A Density Functional Theory Study on the Mechanism of Complete Ethanol Oxidation on Ir(100): Surface Diffusion-Controlled C–C Bond Cleavage. *J. Phys. Chem. C* **2020,** *124* (49), 26953-26964.

36. Bader, R. F. W., A quantum theory of molecular structure and its applications. *Chem. Rev.* **2002,** *91* (5), 893-928.

37. Henkelman, G.; Arnaldsson, A.; Jónsson, H., A fast and robust algorithm for Bader decomposition of charge density. *Computational Materials Science* **2006,** *36* (3), 354-360.